10TH INTERNATIONAL SYMPOSIUM ON PARTICLE IMAGE VELOCIMETRY - PIV13
Delft, The Netherlands, July 1-3, 2013

Examination of turbulence structures in the bottom boundary layer of the coastal ocean by submersible 3D-PTV

Edward Steele[1], **Alex Nimmo-Smith**[1], **Andrey Vlasenko**[2], **Vasyl Vlasenko**[1] **and Phil Hosegood**[1]

[1] School of Marine Science & Engineering, Plymouth University, Plymouth, U.K.
edward.steele@plymouth.ac.uk

[2] Max Planck Institute for Meteorology, Hamburg, Germany

ABSTRACT

The three-dimensional turbulence structures in the bottom boundary layer of the coastal ocean are examined by submersible 3D-PTV. The system consists of four high-resolution digital cameras that view a 20x20x20 cm^3 sample volume illuminated by four underwater lights. We outline a new Physics-Enabled Flow Restoration Algorithm (PEFRA), specifically developed for the denoising of highly sparse Particle Image Velocimetry (PIV) and Particle Tracking Velocimetry (PTV) data and discuss the corresponding velocity distributions yielded. These new three-dimensional measurements lend support to the concept that the bottom boundary layer of the coastal ocean comprises packets of hairpin vortices.

1. INTRODUCTION

The rotational, eddying and dynamic motions implied by the name “turbulence” are the dominant state of fluid movement on Earth. As such, turbulence in effective in the transferal of heat and momentum in the sea, as well as dispersing, straining and stressing both particles and living matter in the water column, while diluting and stirring its chemical constituents. A detailed understanding of turbulence is therefore critical to explaining all marine processes and for the development of models that allow us to plan the sustainable exploitation of the marine system.

In shallow seas in particular, turbulence is generated intermittently close to the sea-bed, but little is known of its structure and evolution through the water column. On reaching the surface of well-mixed waters, bottom-generated boils (areas of local upwelling and associated eddies) impact on the dispersion of pollutants, and contribute to the replacement of surface waters from depth [1]. The energy containing turbulence of boundary layer flows consists of coherent packets of “hairpin vortices”, as highlighted in numerical models and laboratory measurements, e.g. [2, 3]. Two-dimensional flow-visualization methods have recently shown that vortical structures also exist in the bottom boundary layer of tidal flows [4, 5, 6, 7]. Conditional sampling based on vorticity reveal that such structures are the key sites within the flow where energy is extracted from the mean flow into turbulence. However, questions remain as to the full three-dimensional form of these essential structures that may, eventually, grow into the depth-scale boils observed at the sea surface.

This work is based on measurements using a submersible Three-Dimensional Particle Tracking Velocimetry (3D-PTV) system, deployed on the east side of Plymouth Sound, Plymouth, U.K. on 9 June 2005 in $\sim$12 m deep water. The center of the sample volume was set at the height of of 0.5 m above the sea-bed. This 3D-PTV system is outlined in the next section, while a new algorithm for the denoising of these flows (applicable to both PIV and PTV measurements) is discussed in Section 3. Section 4 presents the three-dimensional flow structures in the bottom boundary layer of the coastal ocean and corresponding Reynolds Stress statistics.

2. INSTRUMENTATION

The submersible 3D-PTV system is described fully by Nimmo-Smith [8]. It uses four high-resolution digital cameras (1004x1002 pixels, 8 bit) to view a 20x20x20 cm ^{3} sample volume illuminated by four 500 W underwater lights. Electrical power is supplied from a surface support vessel using an umbilical cable. The umbilical also enables communication with the 3D-PTV master computer, that synchronizes the triggering of the cameras at the rate of 25 Hz. Data from each of these cameras are recorded by its own computer, each with 2x400 GB of hard disk storage (3.2 TB total). All underwater components are mounted on a rigid frame. A vane attached to the frame align it at an angle to the mean flow to prevent the contamination of the sample volume by the wake of the system. This alignment is monitored by an Acoustic Doppler Velocimeter (ADV) that also offers auxiliary turbulence statistics at the same height as the sample volume.

After the calibration of the system ([9]), data processing is completed in three stages using the specialist “Particle Tracking Velocimetry” software developed by Maas [10] and Willneff [11]. Firstly, particles are identified in camera frames using a high-pass filter, threshold, segmentation and weighted centroid methods. The application of minimum and maximum size conditions reduces the risks of contamination by noise or large objects. The correspondences between each pair of tracers (from each of the exposures) are then made using parameters from the calibration, to yield three-dimensional distributions of particles at each time step. Finally, tracking is done in image and object space, running the sequence in both directions to maximize the possible linkages between successive frames, and the velocity of each of the particles at each time step is established using a low-pass filter / moving cubic spline [12]. Here, unlike laboratory measurements where small neutrally-buoyant particles are seeded within the flow, plankton and suspended sediments are used as tracers. The inhomogeneous distributions of these sparse, unevenly-shaped particles causes a corresponding increase in the noise level, that complicates the analysis. In these cases especially, using a physics-enabled flow restoration is deemed highly beneficial.

3. FLOW RESTORATION

The new Physics-Enabled Flow Restoration Algorithm (PEFRA) was specifically developed on the basis of the Physically-Consistent and Efficient Variational Denoising (PCEVD) algorithm and uses the weak form of the hydrodynamical equations to penalize unwanted attributes of the input data [13, 14]. Unlike many existing denoising algorithms, PEFRA is not dependent on types of flow, noise or corruptions. The mathematical background to PEFRA is discussed by Vlasenko et al. [15]. Briefly, the algorithm is based on the variational and gradient-descent methods and uses the Vorticity Transport Equation (VTE) for the denoising of fluid flows. At each iteration, it generates new solutions of the VTE that are nearer, in terms of the L2 norm, to the corrupt data than that of the last. The process repeats until the conditions for the algorithm termination are met. This is implemented in four stages. Firstly, the size of the sample volume is increased such that if motions of any turbulence level occur within its middle, they diminish at its boundary. At the extremes of the volume the flow may, thus, be considered linear and the corresponding vorticity flux almost constant, allowing the open boundary conditions to be set. All empty grid-points are then filled by data interpolation / extrapolation and the flow field is then Gaussian-filtered to remove any sharp junctions. A laminar flow field is used as the basis for the (later) restoration. Here, the flow field from the last step is recast such that it is nearer, in terms of the L2 norm, to the vorticity pattern of the laminar flow field corresponding to the input PTV data. This flow field is then modified to fit the recorded velocity distributions, gaining the necessary turbulence level. This reduces the time needed for the flow restoration and the risks of accumulations of numerical errors and is therefore preferred to the direct fitting to the Gaussian velocity data. Finally, the full flow restoration is achieved by minimizing the difference between the input and output velocity data, enforced by the VTE.

The assessment of the algorithm performance with sparse, modeled data (where exact solutions are known) is shown by Vlasenko et al. [15]. Such tests established that this method is able to successfully restore corrupted PIV and PTV measurements, even when missing large sections of data. We will, therefore, only comment on its application to the submersible 3D-PTV measurements and justify any corrections in situ.

The PTV data is validated on a regular grid. Only the nearest node to each of the detected particles are filled by linear interpolation, and the value of all the others set to zero, to minimize the noise that arises from gridding. Figure 1 presents the instantaneous flow structure under conditions typical of a weak eddy, with little organization or with scales less than the 3D-PTV resolution. The usable number of seed-points for the new Physics-Enabled Flow Restoration Algorithm (PEFRA) here is 98. Figure 1a presents the average angle difference, AAD, and the average speed difference, ASD, between the input and output flow field at each of these seed-points, as quantified on a particle-by-particle basis, after the application of PEFRA. The vectors are aligned by the instantaneous velocity (U, V and W in the X, Y and Z directions, respectively), with the colors and scales of these markers being set by the AAD and ASD in turn. The largest of these adjustments occur at the outermost seed-points. The corresponding velocity distributions that have been corrected by PEFRA are shown in Figure 1b. The instantaneous sample volume mean velocity components have been subtracted from each of the vectors to reveal the three-dimensional structure of the turbulence. This is similar to the general structure of the flow shown in Figure 1c, where PEFRA was not applied. Note the difference between the two is seen in the in-filled velocity slice shown at $Z = -10$, that arises from this being the lower boundary of the PEFRA volume (mostly beyond the outermost seed-points), where the algorithm is unconstrained. Figure 2 presents the instantaneous flow structure with a higher turbulence level than that shown in Figure 1. The format of each of the panels (a to c) is the same as for the last figure, with 101 usable seed-points. An increase in the AAD and ASD on a particle-by-particle basis is clearly visible (Figure 2a), with more adjustments seen in the corresponding velocity distributions that have been corrected by PEFRA (Figure 2b) compared to the output where PEFRA was not applied (Figure 2c). Unlike the corrections in Figure 1, where this is mostly limited to the outermost seed-points, the flow field in the middle part of the sample volume in Figure 2 is also more-substantially modified. While possible causes of this difference will be identified, the exact flow field is unknown, as the input comprises sparse in situ data. The original image containing a record of each of the particles enables us to establish whether such a difference arises from individual tracer attributes (e.g. bubbles, large or heavy particles) that affect the final velocity measurements. Figure 3 presents three subsections from the image, viewed from each of the four different camera angles. Within the convex hull of the seed-points, the magnitude of these adjustments resemble individual tracer attributes. Examination of the original image corresponding to the maximum AAD (3.8700) and ASD (0.7845) within the middle part of the PEFRA volume ($-3<X<+3$) reveal this to be a long, thin structure with a major axis of 12.6 mm in Figure 3a. Such particles increase the noise level and thus need adjustments by PEFRA. The particles nearest the grid-points corresponding to the minimum AAD (1.0246) and ASD (0.0245) within the middle part of the PEFRA volume are shown in Figure 3b and Figure 3c, respectively. Here the two particles lie within the convex hull of the seed-points and, being round and small, this lack of adjustments is consistent with the reasoning that they will not affect the noise level as much as larger particles.

4. FLOW STRUCTURE

As with past in situ 2D-PIV measurements (e.g. [6, 7]), different flow conditions were seen to occur in the bottom boundary layer of the coastal ocean. Examination of the flow structures within the 3D-PTV sample volume reveal these mostly comprises quiescent conditions (e.g. Figure 1), punctuated by infrequent "gusts" of large-scale vortical structures (not shown). These gusts remain spatially coherent for at least the time that they are advected within the sample volume. The analysis of such vortices ([16]) suggests an interpretation in line with the view of the boundary layer consisting of coherent packets of hairpin vortices. Here, the most common

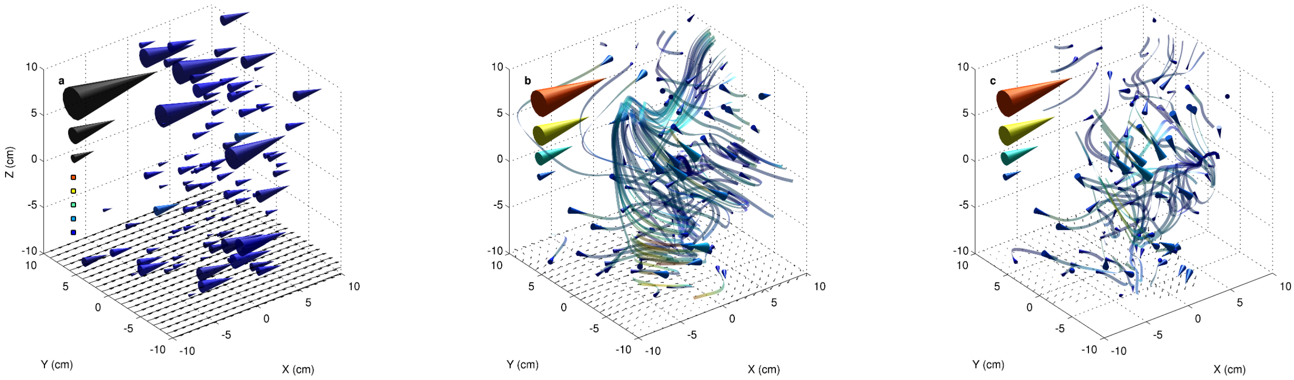

Figure 1: The instantaneous flow structure under conditions typical of a weak eddy. (a) The average angle difference, AAD, and the average speed difference, ASD, between the input and output flow field at each of the seed-points, as quantified on a particle-by-particle basis. The vectors are aligned by the instantaneous velocity. The reference colors are for AAD = 5, 4, ..., 1 (top to bottom) and the black reference vectors are for ASD = 1, 0.50, 0.25 (top to bottom). (b) The corresponding velocity distributions corrected by PEFRA. The instantaneous sample volume mean velocity components have been subtracted from each of the vectors and stream ribbons, starting at the vector locations and colored by the velocity magnitude, reveal the three-dimensional structure of the turbulence. (c) The corresponding velocity distributions not corrected by PEFRA. The reference vectors for both these velocity distributions are for 3, 4, ... 1 cm/s (top to bottom).

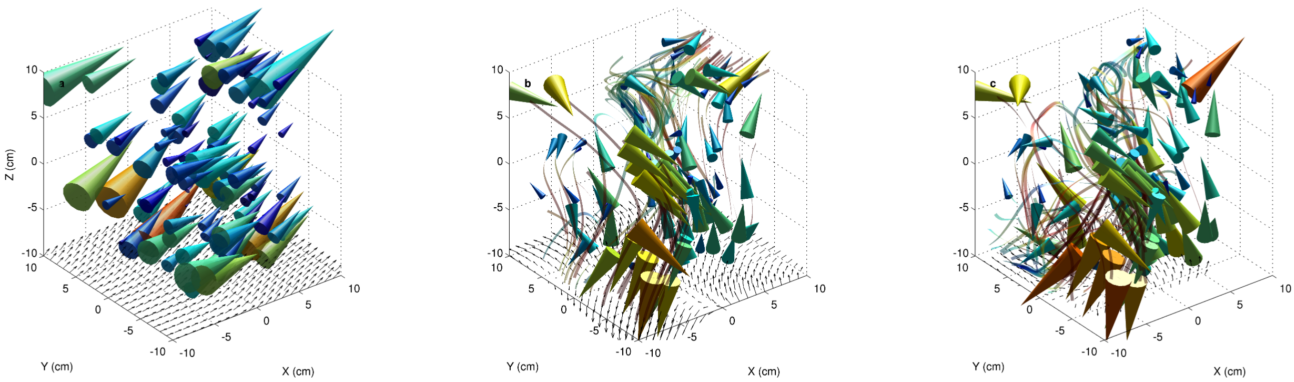

Figure 2: The instantaneous flow structure with a high turbulence level. The visualization process and the reference colors / scales is as per Figure 1.

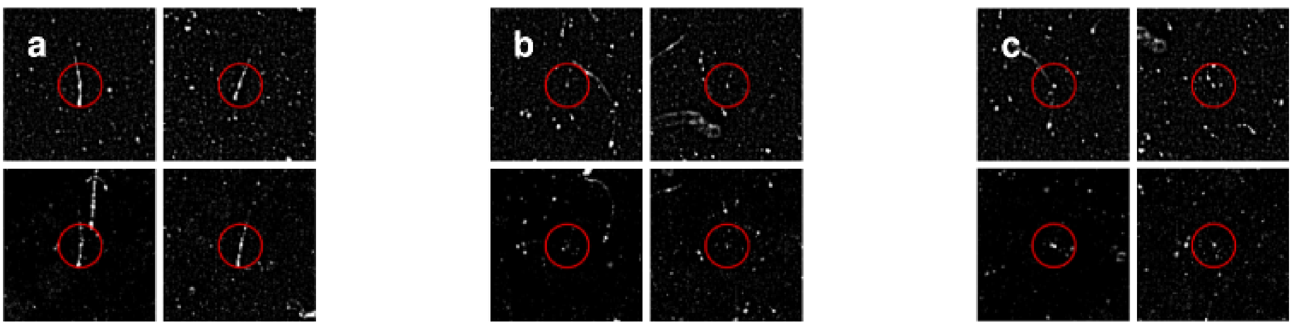

Figure 3: Three subsections from the 3D-PTV image (a to c), viewed from each of the four different camera angles. The particles nearest the grid-points corresponding to: (a) the middle-volume maximum AAD and ASD; (b) the middle-volume minimum AAD; and (c) the middle-volume ASD are highlighted.

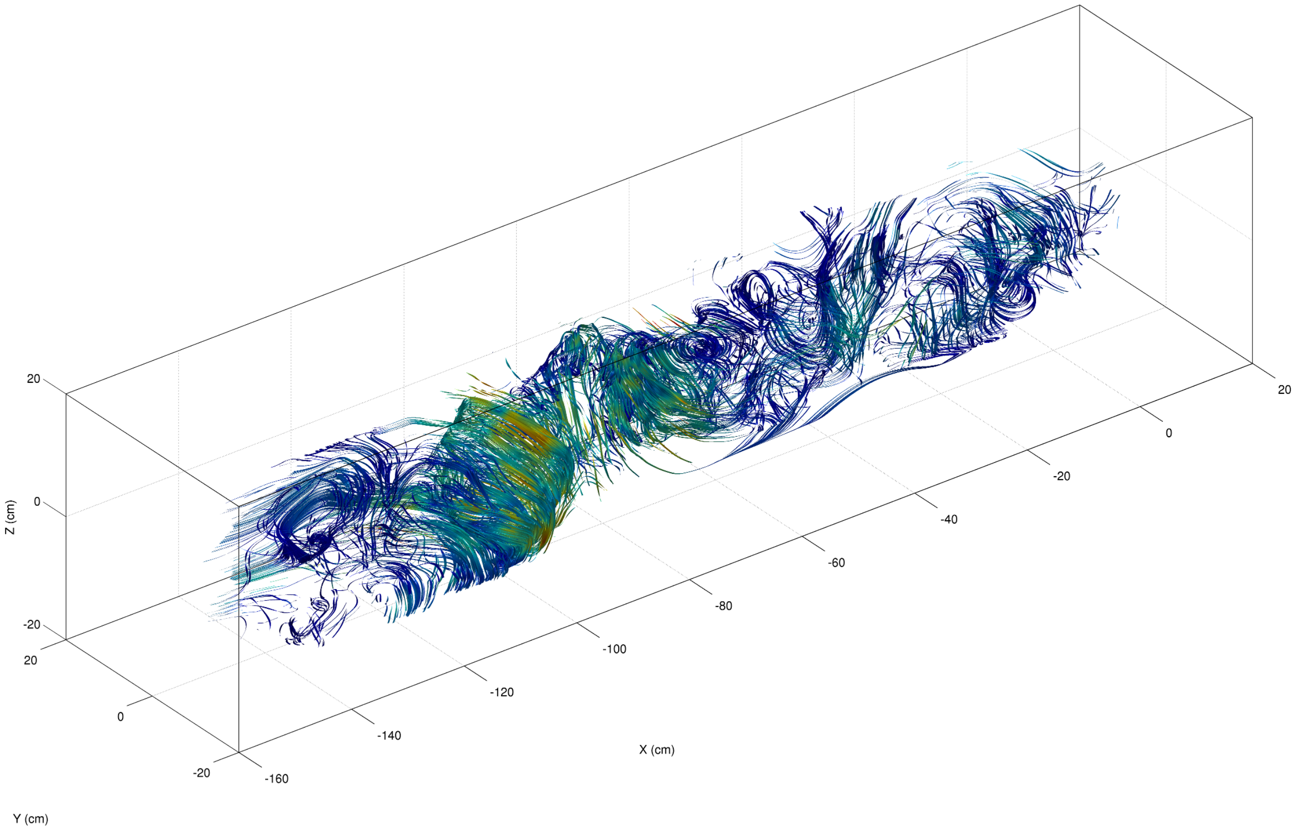

Figure 4: Flow structure within an extended volume created using Taylor's Hypothesis and offsetting the velocity distributions by the mean velocity and the sample interval. The colors of the stream ribbons is as per Figure 1 and Figure 2.

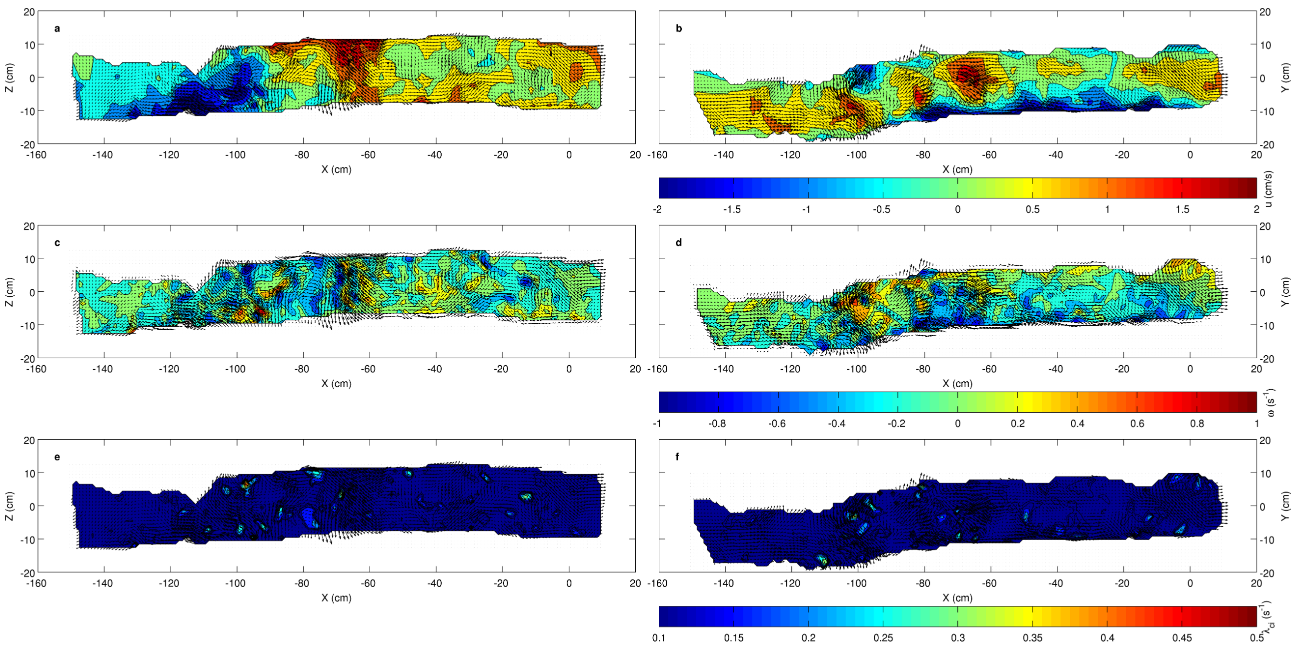

Figure 5: A vertical (a, c, e) and horizontal (b, d, f) section of the same flow shown in Figure 5, corresponding to the along-stream component of the velocity fluctuation, u (a and b), the vorticity, ω (c and d) and the swirling strength, λ_{ci} (e and f). All the panels are overlaid with vectors of the 2D velocity fluctuation ($\{u,w\}$ and $\{u,w\}$) for the respective axes.

of these structures is aligned cross-stream, with the characteristic positive vorticity typical of the "head" of a hairpin. Some of these vortices have a bent core with the upper part similar to a "neck" component and the along-stream lower part inclined to the horizontal. This lower part is consistent with the "legs" of a hairpin – that were also seen to occur individually – with both positive and negative cross-stream vorticity in approximately equal number. Again in agreement with theory, shear (e.g. Figure 2) is seen to exist within a proportion of these flows, that arises from the vertical profile of the boundary layer or the passage of large-scale vortices with a size in excess of that of the 3D-PTV sample volume.

The larger scales of the flow is shown using an application of Taylor's Hypothesis and offsetting the velocity distributions by the mean velocity and the sample interval. Figure 4 presents the corresponding flow field in an extended 0.2x0.2x1.6 m^3 volume, following denoising by PEFRA. A large, inclined, along-stream vortex is clearly visible in the -90<X<-60 cm section, with another, smaller, vortex occurring further upstream (-110<X<-100 cm). These structures are surrounded by more quiescent flow, again with evidence of smaller-scale vortical motions. To facilitate comparisons with other measurements, a vertical (a, c, e) and horizontal (b, d, f) section of the same flow is shown in Figure 5, corresponding to the along stream component of the velocity fluctuation, u' (a and b), the vorticity, ω (c and d) and the swirling strength, λ_{ci} (e and f). All the panels are overlaid with vectors of the 2D velocity fluctuation ($\{u',w'\}$ and $\{u',w'\}$) for the respective axes. The strong negative along-stream component of the velocity fluctuation is consistent with the low-momentum / backward flow typical of the inner part of hairpin vortex packets, around which the coherent structures are seen [17]. In agreement with Dennis [18] and Dennis & Nickels [19, 20], we note that these seem to occur more as component parts, such as asymmetric canes, heads, legs and three-quarter arches, rather than "complete" hairpin vortices. It is concluded these new three-dimensional measurements lend support to the concept that the bottom boundary layer of the coastal ocean comprises coherent packets of such structures (previously referred to as "gusts"), however it is possible that a different analysis will lend support to other theoretical models.

Parametrization of bottom boundary layer turbulence, via the covariance of Reynolds stress, is critical for the numerical modeling of ocean flows. In addition to the visualization of vortices, these three-dimensional measurements allow the three components of the Reynolds stress ($\overline{u'w'}$, $\overline{u'v'}$ and $\overline{v'w'}$) to be estimated, shedding light on the corresponding statistical attributes of the turbulence. Following the methods suggested by Trowbridge [21] to overcome biases that arises from uncertainty in sensor-alignment to flow caused by surface waves, these are calculated from the covariance of the velocity difference between two positions separated by the distance, r:

$$D_{ij} = \overline{[u_i(x+r) - u_i(x)][u_j(x+r) - u_j(x)]} \tag{1}$$

where $i, j = 1, 2, 3$ and are the three velocity components (U, V and W). The magnitude of $D_{ij}(r)$ approaches that of $2\overline{u_i'u_j'}$ when r is larger than the integral scale of the turbulence, I, and much smaller than the wavelength of the surface waves, λ. Examples of these distributions are shown in Figure 6. Future work will apply conditional sampling to these second order structure functions, based on the vortex alignment. Note that differencing between the ADV and 3D-PTV sample volumes will be necessary for the $I < r << \lambda$ conditions to be achieved.

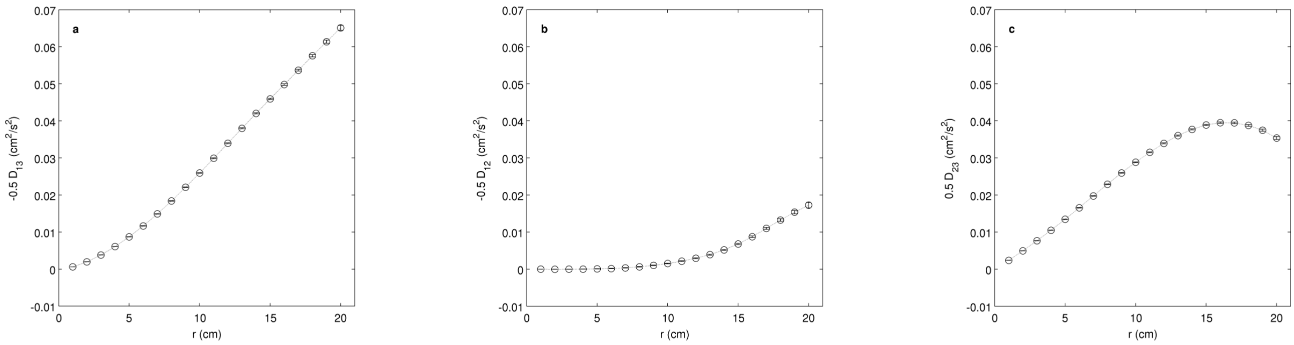

Figure 6: Distributions of: (a) $D_{13}(r)$; (b) $D_{12}(r)$; and (c) $D_{23}(r)$ for the interpolated 3D-PTV data (PEFRA not applied). Note that differencing between the ADV and 3D-PTV sample volumes will be necessary for the $I < r << \lambda$ conditions to be achieved.

5. CONCLUSIONS

The submersible 3D-PTV system, developed by Nimmo-Smith [8], was deployed on the east side of Plymouth Sound, Plymouth, U.K. in $\sim$12 m deep water, with the center of the sample at a height of 0.5 m above the sea-bed. Naturally-occurring plankton and suspended sediments are used as tracers, however, the inhomogeneous distributions of these sparse, unevenly-shaped particles causes a corresponding increase in the noise level and complicates the analysis. It is with this in mind the new Physics-Enabled Flow Restoration Algorithm (PEFRA) was developed. Consistent with the assessment of the algorithm performance with sparse, modeled data (where exact solutions are known) discussed by Vlasenko et al. [15], the corrections made to the recorded in situ flow field are seen to be both necessary and justifiable. The application of the new method to the 3D-PTV measurements allow us to shed light on the dynamical phenomena (i.e. hairpin vortices) that are responsible for the statistical attributes of ocean flows, traditionally recorded by standard instrumentation or modeling.

ACKNOWLEDGMENTS

E. Steele is funded by the School of Marine Science & Engineering, Plymouth University, Plymouth, U.K. Development of the 3D-PTV system was funded by the Royal Society, the Nuffield Foundation and the U.K. Natural Environment Research Council (NE/D000221). The method for the denoising of fluid flows – pioneered by A. Vlasenko & C. Schnorr at the University of Heidelberg, Germany – was adapted under a visiting fellowship award from the Plymouth University Marine Institute, Plymouth, U.K. We are grateful to C. Bunney, E. Davies and D. Uren for assistance with deployment of the 3D-PTV system.

REFERENCES

[1] Nimmo-Smith WAM, Thorpe SA and Graham A, "Surface effects of bottom generated turbulence in a shallow tidal sea", Nature 400 (1999) pp. 251-254.

[2] Zhou J, Adrian RJ, Balachandar S and Kendall TM, "Mechanisms for generating coherent packets of hairpin vortices in channel flow", Journal of Fluid Mechanics 387 (1999) pp. 353-396.

[3] Adrian RJ, Meinhart CD and Tomkins CD, "Vortex organization in the outer part of the turbulent boundary layer", Journal of Fluid Mechanics 422 (2000) pp. 1-54.

[4] Bertuccioli L, Roth GI, Katz J and Osborn TR, "A submersible particle image velocimetry system for turbulence measurements in the bottom boundary layer", Journal of Atmospheric and Oceanic Technology 16 (1999) pp.1635-1646.

[5] Doron P, Bertuccioli L, Katz J and Osborn TR, "Turbulence characteristics and dissipation estimates in the coastal ocean bottom boundary layer from PIV data", Journal of Physical Oceanography 31 (2001) pp. 2108-2134.

[6] Nimmo-Smith WAM, Atsavapranee P, Katz J and Osborn TR, "PIV measurements in the bottom boundary layer of the coastal ocean", Experiments in Fluids 22 (2002) pp. 962-971.

[7] Nimmo-Smith WAM, Katz J and Osborn TR, "On the structure of turbulence in the bottom boundary layer of the coastal ocean", Journal of Physical Oceanography 35 (2005) pp. 72-93.

[8] Nimmo-Smith WAM, "A submersible three-dimensional particle tracking velocimtery system for flow visualisation in the coastal ocean", Limnology & Oceanography: Methods 6 (2008) pp. 96-104.

[9] Svoboda T, Martinec D and Pajdla T, "A convenient multi-camera self-calibration for virtual environments", PRESENCE: teleoperators and virtual environments 14 (2005) pp. 407-422.

[10] Maas HG, Gruen A and Papantoniou D, "Particle tracking velocimetry in three-dimensional flows; part 1: photogrammic determination of particle coordinates", Experiments in Fluids 15 (1993) pp. 133-146.

[11] Willneff J, "A spatio-temporal matching algorithm for 3D particle tracking velocimetry", PhD thesis, Swiss Federal Institute of Technology (ETH) Zurich (2003).

[12] Luthi B, Tsinober A and Kinzelbach W, "Lagrangian measurement of vorticity dynamics in turbulent flow", Journal of Fluid Mechanics, 528 (2005) pp. 87-118.

[13] Vlasenko A, "A physics-based fluid flow restoration method", PhD thesis, University of Heidelberg (2010).

[14] Vlasenko A and Schnorr C, "Physically consistent and efficient variational denoising of image fluid flow estimates" IEEE Transactions of Image Processing 19 (2010) pp. 586-595.

[15] Vlasenko A, Steele E and Nimmo-Smith WAM, "A Physics-Enabled Flow Restoration Algorithm for sparse PIV and PTV measurements", in prep.

[16] Steele E, Nimmo-Smith WAM, Vlasenko A, Vlasenko V and Hosegood P, "Three-dimensional turbulence structures in the bottom boundary layer of the coastal ocean", in prep.

[17] Adrian RJ, "Hairpin vortex organization in wall turbulence", Physics of Fluids 19 (2007) pp. 1-6.

[18] Dennis DJC, "The structural building blocks of turbulent wall-bounded flow", PhD thesis, Cambridge University (2010).

[19] Dennis DJC and Nickels TB, "Experimental measurement of large-scale three-dimensional structures in a turbulent boundary layer; part 1: vortex packets", Journal of Fluid Mechanics 673 (2011) pp. 180-217

[20] Dennis DJC and Nickels TB, "Experimental measurement of large-scale three-dimensional structures in a turbulent boundary layer; part 2: long structures", Journal of Fluid Mechanics 673 (2011) pp. 218-244.

[21] Trowbridge JH, "On a technique for measurement of turbulent shear stress in the presence of surface waves", Journal of Atmospheric and Oceanic Technology 15 (1998) pp. 290-298.